Landscape structure and dispersal rate drive large scale catastrophic shifts in spatially explicit metapopulations

Camille Saade, Emanuel A Fronhofer, Benoit Pichon, Sonia Kéfi

Landscape structure and dispersal rate drive large scale catastrophic shifts in spatially explicit metapopulations

Camille Saade[*,1], Emanuel A. Fronhofer[1], Benoît Pichon[1,2], and Sonia Kéfi[1,3]

[1]ISEM, CNRS, Univ. Montpellier, IRD, EPHE, Montpellier, France

[2]École Normale Supérieure, 45 rue d'Ulm, 75005 Paris, France

[3]Santa Fe Institute, 1399 Hyde Park Road, Santa Fe, NM 87501, USA

[*]**Corresponding author:** camille.saade@umontpellier.fr

Running title: Catastrophic shifts in explicit landscapes

Keywords: metapopulation, space, bistability, catastrophic shifts, hysteresis

Type of article: Letter

Abstract word count: 134 words

Main text word count: 4991 words

Number of references: 50

Figures: 6; **Supplementary Figures:** 12 ; **Supplementary Tables:** 1

Author contributions: C.S., E.A.F., B.P. and S.K. conceived the study. C.S. and B.P. wrote the model and conducted the simulations. C.S. conducted the mathematical analysis of a two patch system. C.S., E.A.F. and S.K. wrote the manuscript and all authors commented on the draft.

Data availability: Code is available on GitHub via Zenodo: https://doi.org/10.5281/zenodo.5705432

Conflict of interest disclosure: The authors of this article declare that they have no financial conflict of interest with the content of this article.

Abstract

Even when environments deteriorate gradually, ecosystems may shift abruptly from one state to another. Such catastrophic shifts are difficult to predict and reverse (hysteresis). While well studied in simplified contexts, we lack a general understanding of how catastrophic shifts spread in realistic spatial contexts. For different types of landscape structure, including typical terrestrial modular and riverine dendritic networks, we here investigate landscape-scale stability in metapopulations made of bistable patches. We find that such metapopulations usually exhibit large scale catastrophic shifts and hysteresis, and that the properties of these shifts depend strongly on metapopulation spatial structure and dispersal rate: intermediate dispersal rates and a riverine spatial structure can largely reduce hysteresis size. Interestingly, our study suggests that large-scale restoration is easier with spatially clustered restoration efforts and in populations characterized by an intermediate dispersal rate.

2

Introduction

As humans exert increasing pressures on ecosystems, understanding how they respond in terms of biomass, species diversity and composition is one of the most pressing issue in ecology. Importantly, some ecosystems can exhibit abrupt responses to gradual changes in environmental conditions (Noy-Meir, 1975; May, 1977; Scheffer et al., 2001). Such responses, referred to as "catastrophic shifts", are usually attributed to the existence of multiple stable ecosystem states between which ecosystems can shift following a perturbation or when a threshold in environmental condition, or "tipping point" is passed (Suding et al., 2004; Kéfi et al., 2007b, 2016). Reverting the ecosystem to its initial state after a shift can be challenging if not impossible, a phenomenon known as "hysteresis". Catastrophic shifts have been described in various ecosystems all over the world (Biggs et al., 2018). Common examples include the eutrophication of shallow lakes (Scheffer et al., 1993; Meijer et al., 1994; Scheffer et al., 1997; Carpenter et al., 1999; Jeppesen et al., 1999), the degradation of coral reefs (Done, 1992; Knowlton, 1992; McCook, 1999; Nyström et al., 2000), the transitions between woodlands and savannas (Dublin et al., 1990; Wilson and Agnew, 1992; Walker, 1995) and the desertification of grasslands (Kassas, 1995; Rietkerk et al., 1997; Nicholson, 2000; Wang and Eltahir, 2000; Reynolds et al., 2007; Kéfi et al., 2007a). Because they are difficult to predict and reverse (Scheffer and Carpenter, 2003) and because they can negatively affect human livelihoods (Reynolds et al., 2007; Biggs et al., 2018), catastrophic shifts have gained a large interest in the literature, providing us with a theoretical framework rooted in bifurcation theory to describe the most common catastrophic shifts (*e.g.*, desertification: Noy-Meir 1975; May 1977; Rietkerk and van de Koppel 1997; Klausmeier 1999; Kéfi et al. 2007b,a; or shallow lakes eutrophication: Scheffer et al. 2001; Carpenter et al. 1999).

However, early theoretical work on catastrophic shifts mainly focused on isolated systems (but see Keitt et al., 2001; van Nes and Scheffer, 2005). Real ecosystems are networks of connected entities between which matter and energy can flow (Leibold et al., 2004). This means that if one of these entities experiences a catastrophic shift locally, this shift can spread through the spatial network and possibly trigger other shifts. Scaling up our understanding of catastrophic shifts from the local

3

scale to the regional scale remains a challenge. In particular, whether local multistability implies regional multistability or whether different stable states can coexist in space (spatial multistability) and how this is modulated by a landscape's spatial structure are still open questions. Recent studies have started to address these questions by including space explicitly in models, under two main settings: *i*) in continuous space, which is well suited to relatively homogeneous habitats where clear spatial entities are not easily identified (see the example of Lake Veluwe in van de Leemput et al., 2015), and *ii*) in discrete space, better representing habitats with clear spatial entities (or patches) connected through dispersal of individuals and flows of resources (e.g., an archipelago such as the Åland Islands in Hanski et al., 1995). As a consequence of these recent developments, we have a good understanding of how locally bistable dynamics can affect the regional behaviour of spatially structured ecosystems: alternative stable states are not expected to coexist in space (Keitt et al., 2001; van de Leemput et al., 2015), unless dispersal is low and space is discrete (Keitt et al., 2001), or strong stochasticity and heterogeneity are at play (van Nes and Scheffer, 2005; Martín et al., 2015). A spatially structured system will experience sharp transitions between fully occupied and fully empty states. These can usually not be called catastrophic shifts as regional bistability and hysteresis are largely reduced due to the dominance of a single of the two possible stable states (Keitt et al., 2001; Hilt et al., 2011; van de Leemput et al., 2015). However, all studies so far assume overly simplified spatial structures, either 1-D (Keitt et al., 2001; van de Leemput et al., 2015) or 2-D continuous space (Martín et al., 2015), linear (Keitt et al., 2001; Hilt et al., 2011) or grid-like (van Nes and Scheffer, 2005) discrete systems. This implies that we currently don't know how more realistic spatial settings affect landscape-scale stability. Indeed, in real ecosystems, suitable habitat is usually neither continuous nor organized on a regular lattice but has a particular structure: terrestrial populations, for example, usually show emergent modularity (Gilarranz, 2020) while riverine systems are typically dendritic (Carraro et al., 2020; Rinaldo et al., 2020). Importantly, these specific spatial configurations have been shown to affect ecological dynamics (Gilarranz et al., 2017; Altermatt and Fronhofer, 2018; Carrara et al., 2012). This omission of spatial complexity is an important shortcoming of the current state of the literature as the properties of such habitats may

4

change how local bistability affects regional scale dynamics and equilibria (van Nes and Scheffer, 2005; van de Leemput et al., 2015).

Here, we aim to fill this gap by studying how local bistability affects the regional scale dynamics of spatially complex populations, using a metapopulation framework in which local patches are connected to each other via dispersal of individuals. We simulate the dynamics of metapopulations with various spatial structures, ranging from classical abstract structures (lattice and random, Erdős–Rényi, spatial networks) to structures rooted in real systems (Random Geometric Graphs for terrestrial systems and Optimal Channel Networks for riverine systems; Gilarranz, 2020; Carraro et al., 2020). For a range of dispersal rates, we measure the size of hysteresis and the position of tipping points at the scale of the whole landscape. We also study how the structure of perturbations themselves affects landscape dynamics by conducting targeted local perturbations of firstly high-degree patches *vs.* low degree patches and secondly neighboring patches *vs.* independent patches.

Model description

Metapopulation model

We used a model of a spatially structured metapopulation describing the dynamics of n patches linked by the dispersal of individuals. Here is a short description of the model, but see the supplement S1 for a more in-depth presentation. The dynamics of the vector $\overrightarrow{x}$ (containing the local biomasses x_i) are described by a system of n coupled differential equations, which can be written in a matricial form:

$$\frac{d\overrightarrow{x}}{dt} = r\overrightarrow{x}\left(1 - \frac{\overrightarrow{x}}{K}\right) - B\frac{\overrightarrow{x}}{A + \overrightarrow{x}} + \mu\, M\overrightarrow{x} \tag{1}$$

The first two terms of Eq. 1 describe the local dynamics of the biomass, while the last term describes the dispersal between patches.

Local dynamics   We describe the local dynamics using a model derived by Noy-Meir (1975) in which plants grow logistically with a growth rate r and carrying capacity K, and are harvested

5

by a fixed consumer with a Holling type II functional response (B: maximal harvesting rate, A: half saturation constant). For the rest of this work, we used the same fixed values for r, K and A (Table S6.1). These parameter values give rise to two tipping points at $B = 50$ and $B = 56.25$ between which the system is bistable: it admits two stable equilibria ($x_i = 0$ and $x_i = r_1 > 0$) separated by an unstable equilibrium ($0 < r_2 < r_1$) (Fig. 1a).

Note that this is one of several possible models of bistability that we chose because of its simplicity and intuitive biological interpretation. Importantly, we show in the supplement S3 how this model and three other common models of bistable systems share a common structure through parameter aggregation which highlights the generality of our findings.

Spatial dynamics   We consider that individuals leave their local patch at a constant rate μ and that the dispersing individuals are distributed evenly among adjacent patches. Mathematically, the vector describing net dispersal for all patches is given by the last term of Eq. 1 ($\mu M \vec{x}$) where M is a matrix describing the structure of the landscape: the diagonal terms describe emigration ($M_{i,i} = -1$) and the off-diagonal terms describe the neighbourhood relationship between patches (see detail in supplement S1).

Integration scheme   We simulated the dynamics using the function *ode* (R-package deSolve, version 1.28). We performed linear regressions on the biomass of each patch over the last 100 simulated values to determine whether the metapopulation had reached an equilibrium (slope smaller than 10^{-3}).

Analysis of a two-patch system

Before moving on to large systems which are only accessible through simulation (see section "Landscape design"), we conducted analytically the stability analysis of a simple system for demonstrating general principles. We used a particular case of Eq. 1 with only two patches exchanging biomass at a rate μ (supplement S1: "Two-patch system"). We determined all its existing equilibria as well as

6

their stability using *MatCont* (version 7.2, in *MATLAB R2017b*). 114

Landscape design 115

We used four different types of landscapes (see supplement S2 for more details on landscape 116
generation, and Fig. S6.1 to S6.3 for examples of landscapes): *i*) Regular graphs, where patches 117
are arranged regularly on a lattice with periodic boundary conditions. While not very realistic, 118
such landscapes have been used in previous studies (Keitt et al., 2001; van Nes and Scheffer, 119
2005) and we include them for the sake of comparison. *ii*) Erdös-Rényi graphs are obtained by 120
randomly connecting pairs of patches with a fixed probability p and can be thought of as a null 121
model. *iii*) Random Geometric Graphs (RGGs) are obtained by randomly drawing patch coordinates 122
in space and connecting patches depending on distance. The random distribution of patches in 123
space results in the emergence of modularity which is thought to be characteristic of terrestrial 124
systems (Gilarranz, 2020). *iv*) Optimal Channel Networks (OCNs) are generated by simulating 125
geomorphological processes to obtain a structure closely resembling that of a river (Carraro et al., 126
2020). 127

For each type of landscape, we generated 50 replicates with each $n = 100$ patches. The main text 128
analysis was made on landscapes where patches had on average approximately 4 neighbours (except 129
for OCNs as their generating process constrains their connectivity), and we conducted sensitivity 130
analysis on the connectivity using networks with higher and lower connectivity (supplement S4). 131

Simulations 132

For each type of network, we generated 50 replicates and computed their bifurcation diagram for 133
100 values of dispersal rates (μ) between 0.001 and 1. We used 46 values of harvesting rates (B) 134
equally spaced between 50 and 56.25 (the bistability range of a single patch). For each value of B, 135
we computed the high-biomass (resp. low-biomass) branch of the bifurcation diagram by initially 136
setting each patch to the positive (resp. null) equilibrium of a single patch. Once the system had 137
reached an equilibrium, we degraded (resp. restored) 5% of the patches by setting them to a null 138

7

biomass (resp. to their positive equilibrium). We then measured the steady-state average biomass in   139
order to plot the bifurcation diagram.   140

We used three different perturbation schemes: Firstly, we chose the 5 patches to be de-   141
graded/restored randomly (Fig. 2-4). Secondly, we focused on the influence of node degree   142
by degrading/restoring patches chosen from either the most or least connected nodes (Fig. 5). We   143
conducted these perturbations in Erdös-Rényi graphs, RGGs and OCNs but not in regular graphs (as   144
their nodes all have the same degree). Thirdly, we focused on the influence of the spatial structure   145
of perturbations by degrading/restoring patches that were either clustered or dispersed in space   146
(Fig. 6). In regular graphs, this was done by drawing the 5 perturbed nodes either from a 9 patch   147
neighborhood (3x3 patches in grid landscapes or 9 adjacent patches in circular landscapes) for the   148
"clustered" modality or drawing them from the whole landscape for the "dispersed" modality. In   149
RGGs and OCN, we identified modules using the function *edge.betweenness.community* (R-package   150
igraph version 1.2.6) and the dispersal matrix M, and drew 5 patches from a single modules for the   151
"clustered" modality or from 5 different modules for the "dispersed" modality. We did not conduct   152
this third analysis on Erdös-Rényi graphs as they are not spatially explicit so there is no notion of   153
proximity between patches.   154

Characterizing large scale shifts   155

From the established bifurcation diagrams, we extracted synthetic information on the large scale   156
behaviour of the system.   157

State diagram   We affected one of three categorical states to each simulation depending on its   158
steady-state average biomass: it was considered "fully occupied" when the average biomass was   159
higher than 99% of the pre-perturbation high-biomass equilibrium, "empty" when the average   160
biomass was less than 1% of it and "partially occupied" in between. We constructed state diagrams   161
for each type of networks by averaging the states borders over all replicates and plotting them as a   162
function of the harvesting rate (B) and dispersal rate (μ).   163

8

Hysteresis size We computed the size of the hysteresis as the area in between the higher and 164
lower branches of the bifurcations diagram. 165

Tipping point Finally, we computed the position of the tipping points from the bifurcation 166
diagrams as the value of harvesting rate (B) at which the average biomass decreased (for the 167
degradation trajectory) or increased (for the restoration trajectory) the most. 168

Results
169

Analysis of a two-patch system
170

Starting from an isolated patch exhibiting bistability (Fig. 1a) and connecting it to another patch, we 171
found that, at high dispersal, spatial bistability — the stable coexistence of patches in different states 172
— is not possible and the whole system behaves as a single bistable unit (Fig. 1b, supplement S5). 173
As dispersal decreases, spatial bistability becomes possible as new stable states appear (Fig. 1c, 174
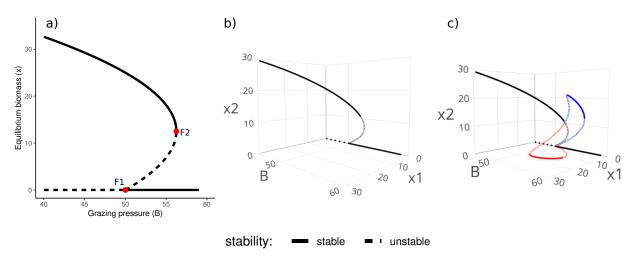supplement S5) with strong differences in biomass between the two patches. 175

Figure 1: Bifurcation diagrams of a single patch (a) and of two patch systems (b, c) at high (b, $\mu = 0.3$) and low (c, $\mu = 0.005$) dispersal rates. Full lines are stable equilibria, dashed lines are unstable equilibria. (a) Equilibria of the biomass (x) of an isolated patch as a function of the grazing pressure (B). (b, c) Equilibria of the biomasses (x_1, x_2) of two patches connected by dispersal, as a function of the grazing pressure (B).

9

Stable states of larger metapopulations

We now focus on larger metapopulations made of 100 patches. The results described in the following sections held qualitatively when considering graphs that were overall more or less connected (see sensitivity analysis in supplement S4).

On a regular grid, a larger metapopulation can reach different states (fully occupied, empty or partially occupied) depending on dispersal (μ) and harvesting (B) rates (Fig. 2). At high dispersal rates (Fig. 2a-d, $\mu > 0.15$), only two stable states are possible: the landscape is either fully occupied (the average biomass is that of a single patch) or empty (the average biomass is null), and the metapopulation is bistable as a whole (regional bistability). The bifurcation diagram of the average biomass is then qualitatively similar to that of a single patch (Fig. 2d), albeit with a displaced restoration tipping point. As dispersal rate decreases, the bistability domain shrinks and partially occupied states (where some of the landscape patches are empty and others are occupied) become stable (*i.e.*, spatial bistability; Fig. 2c, e). At very low dispersal rates, the system behaves roughly as a collection of independent patches: spatial bistability is common, and local degradation (resp. restoration) can neither spread in space nor be reversed. As a consequence, the bifurcation diagram of the average biomass mostly reflects the initial conditions (Fig. 2f).

These results hold qualitatively for other types of landscapes such as Erdös-Rényi and Random Geometric Graphs (RGG), even though spatial bistability is then more common than for regular grids (Fig. 3a-c). In Optimal Channel Networks (OCNs), we observed a similar state space diagram, although the bistability domain was reduced and did not expand much with increasing dispersal rates, and the partially occupied (*i.e.*, spatially bistable) state was stable at higher dispersal rates than for the other networks (up to $\mu \approx 0.25$) (Fig. 3d).

Characterisation of regional scale catastrophic shifts

Hysteresis size   For all landscape types, the hysteresis size of the metapopulation was smaller than that of an isolated patch (Fig. 4a). Hysteresis sizes were similar across network types at low dispersal rates ($\mu < 0.1$) but quickly diverged for higher dispersal rates: regular graphs had the larger
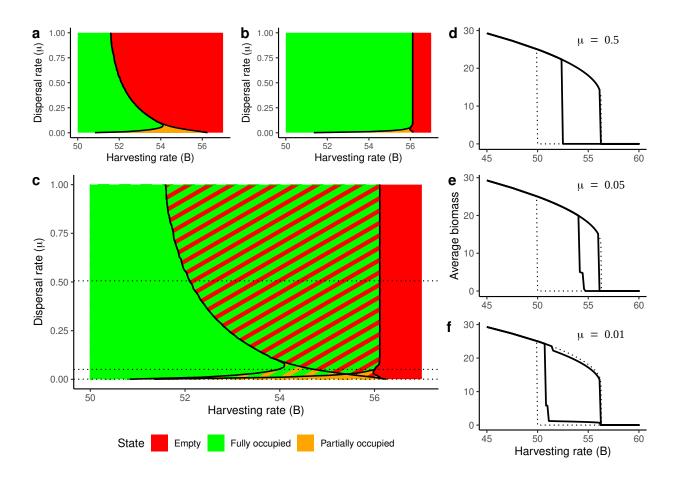
10

Figure 2: State diagram of a regular grid made of 10*10 bistable patches as a function of the harvesting rate (*B*) and the dispersal rate (*mu*) (a, b, c) and bifurcation diagrams of the average biomass for various dispersal rates (d, e, f). **(a) and (b)** state diagrams of a regular grid of 10*10 bistable patches when starting from 5 random occupied patches in a otherwise empty landscape (a) or 5 random empty patches in an otherwise occupied landscape (b). The colors denote the final state of the system: "fully occupied" (green) means that the total equilibrium biomass was greater than 99% of the maximal equilibrium biomass, "empty" means that the total equilibrium biomass was smaller than 1% of the maximal equilibrium biomass, and "partially occupied" means that the system was neither empty nor fully occupied. **(c)** general state diagram of the aforementioned system, obtained by superimposing panels (a) and (b). **(d), (e) and (f)** bifurcation diagrams of the average biomass of a regular grid (10*10 bistable patches) for different dispersal rates ((d): $\mu = 0.5$, (e): $\mu = 0.05$, (f): $\mu = 0.001$). State space limits from panels (a), (b) and (c) were obtained as the average of 50 replicates; panels (d), (e) and (f) are the bifurcation diagram of a single replicate each.

hysteresis size, followed by Erdös-Rényi graphs and RGGs and finally by OCNs, whose hysteresis ²⁰²

size was almost null at high dispersal rates ($\mu > 0.2$). For regular graphs, Erdös-Rényi networks ²⁰³

and RGGs, we found a unimodal relationship between the hysteresis size and dispersal rate: the ²⁰⁴

hysteresis size quickly decreased at first and reached a minimum at $\mu \approx 0.1$ before slowly increasing ²⁰⁵
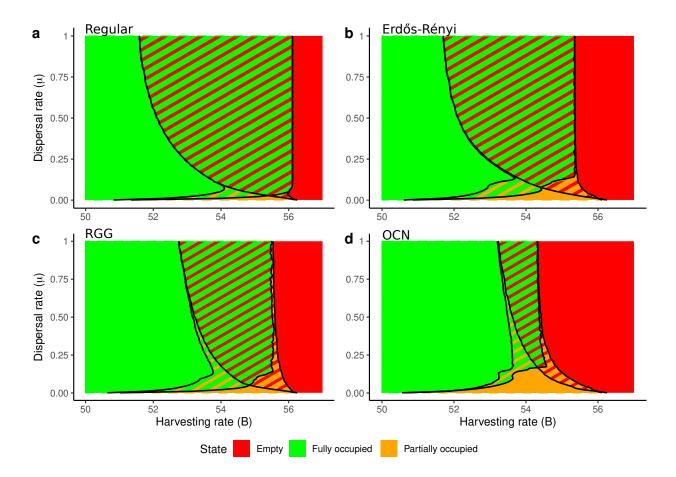
11

Figure 3: State space diagrams of spatially structured metapopulations as a function of the harvesting rate (B) and the dispersal rate (μ) for various types of landscapes: (a) a regular grids (10*10 patches on a torus) (same as fig 2c); (b) Erdös-Rényi graphs; (c) random geometric graphs (RGGs) and (d) optimal chanel networks (OCNs). Each panel was obtained by combining the state space diagram of a landscape starting with 5% of random occupied patches and the state space diagram of a landscape starting with 5% of random empty patches, averaged over 50 replicates, similarly as Fig. 2(a-c).

with the dispersal rate to reach a plateau ($\mu > 0.1$). Hysteresis size in OCNs also decreased with dispersal rate at first, but stayed at a constant value for higher dispersal rates ($\mu > 0.2$).

Tipping points   For all landscape types, the degradation (resp. restoration) tipping points happened at a lower (resp. higher) harvesting rate than in an isolated patch, which explains the lower hysteresis size in spatially structured landscapes (Fig. 4b and c). The degradation tipping point was mostly unaffected by dispersal rate beyond a threshold ($\mu > 0.1$ for regular graphs, Erdös-Rényi graphs and RGGs and $\mu > 0.25$ for OCNs). The restoration tipping point, however, was more affected by dispersal rate (Fig. 4c). Interestingly, this means that the patterns observed for hysteresis size are

12

mainly explained by modifications of the restoration rather than of the degradation point. OCNs were the landscapes whose tipping points were overall the most different from an isolated patch.

Similarly to what was observed for hysteresis size, the tipping points were closer to those of a single patch at low dispersal rates, but then deviated from it before reaching a plateau.
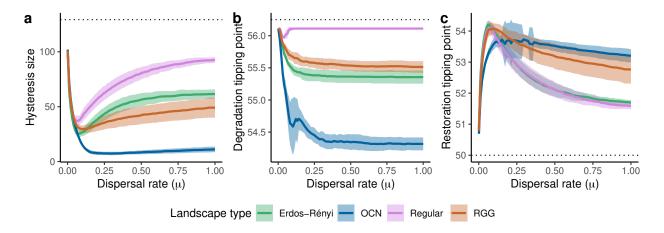

Figure 4: Effect of different landscape types (spatial structures) on the regional dynamics of metapopulations (purple: regular graphs; green: Erdös-Rényi graphs; brown: random geometric graphs (RGGs); blue: optimal channel network (OCNs)). (a) Size of the hysteresis (computed as the area between the upper and lower branches of the bifurcation diagram of the average biomass) as a function of the dispersal rate. (b) and (c) large scale tipping points as a function of the dispersal rate: value of the harvesting rate (B) at which the system loses (b) or gains (c) the most biomass. All quantities are computed as the mean (full line) and standard deviation (colored areas) of 50 replicates.

Perturbation modality and large scale catastrophic shifts

Lastly, we considered how different types of perturbations affected large scale shifts, as opposed to the random perturbations considered up to this point.

Spatial proximity of perturbations Both in regular graphs and RGGs, spatially clustered perturbations resulted in a smaller hysteresis compared to spatially dispersed perturbations (Fig. 5a) for all dispersal rates higher than ~ 0.1. This was once again explained by differences in the restoration tipping point: while degradation happened at the same harvesting rate in both perturbation modalities (Fig. 5b), the restoration happened at higher harvesting rates for clustered perturbations

(Fig. 5c).   226

In OCNs, the spatial organization of perturbations had no effect on the hysteresis size (Fig.5a)   227

as both degradation and restoration were mainly unaffected by the perturbation modality (Fig. 5b)   228

and c).   229
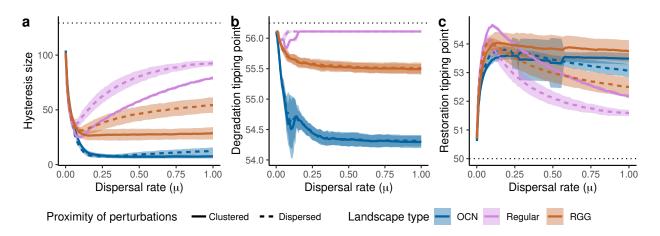

Figure 5: Effects of different perturbation types on the regional dynamics of metapopulations (full line: clustered perturbations, dashed lines: dispersed perturbations) and different landscape types (purple: regular grid; brown: random geometric graphs (RGGs); blue: optimal channel networks (OCNs)). (a) Size of the hysteresis as a function of the dispersal rate. (b) and (c) regional scale tipping points as a function of the dispersal rate: value of the harvesting rate (B) at which the system loses (b) or gains (c) the most biomass. All quantities are computed as the mean (lines) and standard deviation (colored areas) of 50 replicates.

Connectivity of perturbed patches   In RGG, perturbing highly vs. lowly connected patches had   230

no discernible effect on the hysteresis size and tipping points of the metapopulation (Fig. 6). In Erdös- 231

Rényi graphs and OCNs, perturbing lowly connected patches resulted in a slightly smaller hysteresis   232

at high dispersal rates ($\mu > 0.1$) (Fig. 6a), once again because of differences in the restoration point: 233

restoration happened at higher harvesting rate for perturbations of lowly connected nodes compared   234

to highly connected nodes (Fig. 6c), while the degradation point was unaffected (Fig. 6b).   235
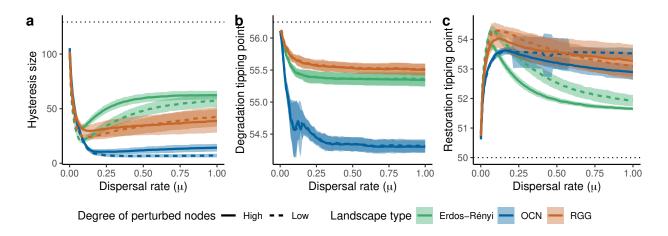
14

Figure 6: Effect of different perturbation types on the regional dynamics of the metapopulation (full line: perturbation of high-degree patches, dashed lines: perturbation of low-degree patches) and different landscape types (green: Erdös-Rényi graphs; brown: random geometric graphs (RGG); blue: optimal channel networks (OCN)). (a) Size of the hysteresis as a function of the dispersal rate. (b) and (c) regional scale tipping points as a function of the dispersal rate: value of the harvesting rate (B) at which the system loses (b) or gains (c) the most biomass. All quantities are computed as the mean (lines) and standard deviation (colored areas) of 50 replicates.

Discussion

Stable states of metapopulations composed of locally bistable patches

We found that the stable states of metapopulations made of locally bistable patches depended strongly on dispersal rate and were qualitatively similar for various spatial structures and network connectivity.

Strong dispersal homogenized biomass over space and drove the system towards one of two stable states: either all the patches were occupied and the average biomass was roughly the same as the positive equilibrium of an isolated patch, or all patches were empty and the average biomass was null. These two states had overlapping stability ranges, making the metapopulation bistable as a whole, with a clear hysteresis and abrupt shifts. Therefore, we expect the local degradation or restoration of a few patches in an otherwise homogeneous metapopulation to be quickly reversed, which means that, in a metapopulation with strong dispersal, local restoration efforts are bound to fail unless the environmental conditions cross a metapopulation-scale tipping point. Once this tipping point is crossed, local restoration efforts should spread in space until the whole metapopulation is

restored.

When dispersal was sufficiently weak, patches were functionally independent from each other. The exchange of biomass was too low for patches to impact the state of their neighbours and spatial bistability was common as occupied and empty patches could thus coexist in space. In our setting, perturbing only 5% of the patches, this resulted in a large scale behaviour very similar to that of a single patch: the unperturbed patches (95% of the landscape) shifted only when the tipping point of an isolated patch was reached, independently of the perturbations. From a conservation standpoint, the effective independence of patches ensures that a local degradation won't spread in space and policies could focus on local measures of protection without worrying about spatial effects. However, in the absence of significant fluxes between patches, spatial heterogeneity and stochasticity should have a strong impact on local dynamics and extinction probability. How this can affect large scale dynamics is still an open question as these processes can synergize in surprising ways: for example, Martín et al. (2015) found that demographic stochasticity coupled with a low dispersal rate results in smooth transition in 1- and 2-dimensional continuous space.

Interestingly, this means that in metapopulations made of locally bistable patches, strong dispersal should raise concerns as it translates into possible regional scale catastrophic shifts with a pronounced hysteresis and little prospect for local restoration. On the other hand, weak dispersal should open the door to local conservation and restoration efforts. This should be taken into account when planning conservation measures such as assisted migration or ecological corridors, as increasing a species dispersal rate could make it prone to large scale catastrophic shifts.

Characteristics of regional scale catastrophic shifts

We observed a smaller hysteresis size than expected from the dynamics of isolated patches for all landscape types. This is particularly pronounced in OCNs where hysteresis was largely reduced (less than $1/10^{th}$ of the hysteresis of a single patch for dispersal rates > 0.2). This was expected from previous studies, which predicted that hysteresis should mostly disappear at high dispersal in one dimensional continuous space (van de Leemput et al., 2015) or in linear metapopulations (Keitt

16

et al., 2001; Hilt et al., 2011). Since OCNs are made of large linear parts, they fit this prediction best. The other types of landscapes have more links per patch on average than OCNs, which diluted the effect of any focal patch on more than two neighbours. As a consequence, a local degradation or restoration in an otherwise homogeneous landscape is less likely to spread to its neighbours and more likely to be reversed than in less connected landscapes, resulting in a larger hysteresis.

Interestingly, this reduced hysteresis compared to an isolated patch is mostly due to an earlier restoration, *i.e.*, restoration was reached at harsher conditions than expected from the local dynamics. This is due to an asymmetry in the bifurcation diagram of local dynamics: the tipping point towards restoration is a transcritical bifurcation (Fig. 1a, point F1), while the tipping point towards degradation is a saddle-node bifurcation (Fig. 1a, point F2). As a consequence, the null biomass equilibrium has a small basin of attraction while the positive equilibrium has a large basin of attraction, even close to its tipping point, so local restorations are more easily spread in space than local degradations. This asymmetry of the basins of attraction holds true for various models of desertification (Rietkerk and van de Koppel, 1997; Klausmeier, 1999); we therefore expect these systems to also exhibit a reduced hysteresis and easier restoration in metapopulations than expected from the dynamics of a single patch. However, it is important to keep in mind that other models of bistability should behave differently. For example, a system with two transcritical bifurcations should show almost no hysteresis, while a system with saddle-node bifurcations should show an hysteresis of similar size to an isolated patch. Interestingly, a system with a transcritical bifurcation for the degradation and a saddle-node bifurcation for the restoration should have an hysteresis size similar to what we find here, but mainly through an earlier degradation.

Hysteresis size was found to vary with dispersal rate. The largest hysteresis size was observed at the lowest dispersal rate ($\mu = 0.001$) for all types of networks, and quickly decreased with dispersal rates. After this initial decrease, the hysteresis size increased with dispersal to a plateau. This means that the smallest hysteresis size and the easiest restoration happened for intermediate dispersal rates ($\mu \approx 0.1$) for which the dispersal is strong enough for a local restoration to affect neighbouring patches, but still sufficiently weak to avoid the dilution of the added biomass in space, triggering a

17

travelling wave of restoration. Interestingly, we observed a large hysteresis size at both very low ${}_{303}$ and high dispersal rates, but with opposite underlying mechanisms: in the case of low dispersal, ${}_{304}$ large scale shifts are hard to induce because local perturbations in a few patches won't affect the ${}_{305}$ neighbouring patches at all. At high dispersal, large scale shifts are also hard to induce, but because ${}_{306}$ local perturbations quickly get diluted across the whole landscape. ${}_{307}$

It is worth noting that these variations with dispersal rate are reminiscent of Zelnik et al. (2019)'s ${}_{308}$ regimes of spatial recovery: local restoration efforts could only spread in space at intermediate ${}_{309}$ dispersal rates (what Zelnik called "rescue recovery"), but not at very low dispersal ("isolated ${}_{310}$ recovery": local restoration does not affect neighbouring patches) or at very high dispersal ("mixing ${}_{311}$ recovery": the local restoration effort is diluted over the whole landscape). ${}_{312}$

Characterizing how hysteresis size varies with dispersal rate is important from a conservation ${}_{313}$ standpoint, because a smaller hysteresis means that it is easier to restore the system after a large ${}_{314}$ scale degradation. We can try to derive broad predictions about which species should raise concern ${}_{315}$ for large scale catastrophic shifts. In terrestrial systems, dispersal increases with height for plants ${}_{316}$ (Tamme et al., 2014) and often with body size for animals (Stevens et al., 2014), while population ${}_{317}$ growth rate is expected to decrease with body mass (Savage et al., 2004). Because of these ${}_{318}$ relationships, we can speculate that one should be more concerned by the possibility of large ${}_{319}$ scale catastrophic shifts in systems dominated by large species. Similarly, oceanic systems may ${}_{320}$ be more prone to large scale catastrophic shifts with a marked hysteresis since oceanic species ${}_{321}$ can exhibit strong propagule dispersal that impacts local dynamics (Kinlan and Gaines, 2003). ${}_{322}$ Of course, dispersal also depends strongly on other species traits (*e.g.*, seed dispersal syndromes, ${}_{323}$ body temperature) and such broad predictions remain speculations and cannot replace the detailed ${}_{324}$ knowledge on a species of interest. ${}_{325}$

The landscape type also affected the metapopulation regional scale behaviour. In OCNs, ${}_{326}$ hysteresis size did not increase with dispersal rates but stayed low after the initial decrease. This ${}_{327}$ is because OCNs are almost one-dimensional, with large linear parts. This linearity limited the ${}_{328}$ aforementioned dilution of local restoration efforts and resulted in tipping points almost unchanged ${}_{329}$

18

by dispersal at high dispersal. On top of that, patches in OCNs have a low average degree, with 330 most nodes having only 1 or 2 neighbours. Because of this, the dispersal from any focal patch was 331 concentrated on a few neighbours. This allowed an easier induction of regional scale catastrophic 332 shifts through a domino effect (even for degradation), as evidenced by the degradation and restoration 333 tipping points happening at respectively lower and higher harvesting intensity than in the other 334 landscape types. Interestingly, two other studies support this result: Hilt et al. (2011) modeled a 335 river as a strictly linear chain of discrete patches and found that hysteresis disappears entirely at 336 high dispersal rates, while Martín et al. (2015) showed that one dimensional systems tend to have 337 smaller hysteresis and smoother transitions than their two (and even three) dimensional counterparts. 338 The other landscape types (grid and RGGs) have no linear parts and an higher average degree 339 (4 neighbours on average). Because of this, the effect of local perturbations was split between 340 several neighbours and diluted in the metapopulation, making it more difficult to induce regional 341 scale shifts and resulting in a larger hysteresis. This was supported by our sensitivity analysis on 342 network connectivity (supplement S4): networks with a smaller average degree (Fig. S4.1) had a 343 smaller hysteresis while networks with a larger average degree (Fig. S4.2) had a larger hysteresis. 344 From these results, we expect large-scale catastrophic shifts with a pronounced hysteresis to be 345 more likely in well-connected and two dimensional systems (*e.g.*, terrestrial systems, open ocean) 346 than in systems that are lowly connected or restricted to large linear stretches (*e.g.*, rivers, coastal 347 ecosystems). 348

Lastly, we explored how the spatial structure of perturbations themselves could affect large scale 349 catastrophic shifts. We found that close-by restoration efforts, *e.g.*, patches from a single module in 350 RGGs, are more likely to induce regional scale restorations and results in a smaller hysteresis size 351 than restoration efforts conducted randomly in space. This is because restoring close-by patches 352 concentrates the added biomass on a smaller area (*e.g.*, the module where we restore patches in 353 RGGs) and limits the dilution of biomass in space. This makes it easier to trigger the large scale 354 restoration of the metapopulation. Studies in continuous space highlight a similar result: van de 355 Leemput et al. (2015) identifies a "minimal size of disturbance to initiate a travelling wave". Several 356

19

disturbances smaller than this size won't initiate a large scale shift as they get diluted individually, $_{357}$ but grouping these disturbances over a single area will initiate a large scale shift. $_{358}$

On the other hand, the connectivity of perturbed patches slightly increased the hysteresis size in $_{359}$ Erdös-Rényi graphs and OCNs, and had surprisingly no effect in RGGs. This is probably because $_{360}$ sampling from low degree patches for the perturbations incidentally results in sampling far away $_{361}$ patches, which partially masks the effect of patch connectivity on hysteresis. $_{362}$

Conclusion $_{363}$

In conclusion, we showed that one can not extrapolate the bifurcation diagram of a single patch $_{364}$ to predict regional scale dynamics. Instead, we highlight that a metapopulation can exhibit large $_{365}$ scale catastrophic shifts and hysteresis, and that the position of its tipping points depends on both its $_{366}$ spatial architecture and its dispersal rate. We find that restoration after a large scale degradation is $_{367}$ easier with *i*) local restoration efforts concentrated on a restricted area and *ii*) intermediate dispersal $_{368}$ rates. Our findings differ markedly from the predictions established on regular one-dimensional $_{369}$ systems and show that we should consider the explicit structure of metapopulations or at least $_{370}$ their properties (dimension, average degree and degree heterogeneity) when trying to predict their $_{371}$ regional scale dynamics. $_{372}$

References

Altermatt, F. and E. A. Fronhofer. 2018. Dispersal in dendritic networks: Ecological consequences on the spatial distribution of population densities. Freshwater Biology, **63**:22–32.

Biggs, R., G. D. Peterson, and J. C. Rocha. 2018. The regime shifts database: a framework for analyzing regime shifts in social-ecological systems. Ecology and Society, **23**:9.

Carpenter, S. R., D. Ludwig, and W. A. Brock. 1999. Management of eutrophication for lakes subject to potentially irreversible change. Ecological applications, **9**:751–771.

Carrara, F., F. Altermatt, I. Rodriguez-Iturbe, and A. Rinaldo. 2012. Dendritic connectivity controls biodiversity patterns in experimental metacommunities. Proceedings of the National Academy of Sciences, **109**:5761–5766.

Carraro, L., E. Bertuzzo, E. A. Fronhofer, R. Furrer, I. Gounand, A. Rinaldo, and F. Altermatt. 2020. Generation and application of river network analogues for use in ecology and evolution. Ecology and Evolution, **10**:7537–7550.

Done, T. J. 1992. Phase shifts in coral reef communities and their ecological significance. Hydrobiologia, **247**:121–132.

Dublin, H. T., A. R. Sinclair, and J. McGlade. 1990. Elephants and fire as causes of multiple stable states in the serengeti-mara woodlands. The Journal of Animal Ecology, pages 1147–1164.

Gilarranz, L. J. 2020. Generic emergence of modularity in spatial networks. Scientific reports, **10**:1–8.

Gilarranz, L. J., B. Rayfield, G. Liñán-Cembrano, J. Bascompte, and A. Gonzalez. 2017. Effects of network modularity on the spread of perturbation impact in experimental metapopulations. Science, **357**:199–201.

Hanski, I., T. Pakkala, M. Kuussaari, and G. Lei. 1995. Metapopulation persistence of an endangered butterfly in a fragmented landscape. Oikos, pages 21–28.

21

Hilt, S., J. Köhler, H.-P. Kozerski, E. H. van Nes, and M. Scheffer. 2011. Abrupt regime shifts in space and time along rivers and connected lake systems. Oikos, **120**:766–775.

Jeppesen, E., M. Søndergaard, B. Kronvang, J. P. Jensen, L. M. Svendsen, and T. L. Lauridsen. 1999. Lake and catchment management in denmark. In The ecological bases for lake and reservoir management, pages 419–432. Springer.

Jeschke, J. M., M. Kopp, and R. Tollrian. 2004. Consumer-food systems: why type i functional responses are exclusive to filter feeders. Biological Reviews, **79**:337–349.

Kalinkat, G., F. D. Schneider, C. Digel, C. Guill, B. C. Rall, and U. Brose. 2013. Body masses, functional responses and predator–prey stability. Ecology letters, **16**:1126–1134.

Kassas, M. 1995. Desertification: a general review. Journal of arid environments, **30**:115–128.

Kéfi, S., M. Holmgren, and M. Scheffer. 2016. When can positive interactions cause alternative stable states in ecosystems? Functional Ecology, **30**:88–97.

Kéfi, S., M. Rietkerk, C. Alados, Y. Pueyo, A. ElAich, V. Papanastasis, and de Ruiter Peter C. 2007*a*. Spatial vegetation patterns and imminent desertification in mediterranean arid ecosystems. nature, **449**:213–217.

Kéfi, S., M. Rietkerk, M. van Baalen, and M. Loreau. 2007*b*. Local facilitation, bistability and transitions in arid ecosystems. Theoretical Population Biology, **71**:267–400.

Keitt, T. H., M. A. Lewis, and R. D. Holt. 2001. Allee effects, invasion pinning, and species' borders. The American Naturalist, **157**:203–216.

Kinlan, B. P. and S. D. Gaines. 2003. Propagule dispersal in marine and terrestrial environments: a community perspective. Ecology, **84**:2007–2020.

Klausmeier, C. A. 1999. Regular and irregular patterns in semiarid vegetation. Science, **284**:1826–1828.

Knowlton, N. 1992. Thresholds and multiple stable states in coral reef community dynamics. American Zoologist, **32**:674–682.

Leibold, M. A., M. Holyoak, N. Mouquet, P. Amarasekare, J. M. Chase, M. F. Hoopes, R. D. Holt, J. B. Shurin, R. Law, D. Tilman, et al. 2004. The metacommunity concept: a framework for multi-scale community ecology. Ecology letters, **7**:601–613.

Mallet, J. 2012. The struggle for existence. how the notion of carrying capacity, k, obscures the links between demography, darwinian evolution and speciation. Evolutionary Ecology Research.

Martín, P. V., J. A. Bonachela, S. A. Levin, and M. A. Muñoz. 2015. Eluding catastrophic shifts. Proceedings of the National Academy of Sciences, **112**:E1828–E1836.

May, R. M. 1977. Thresholds and breakpoints in ecosystems with a multiplicity of stable states. Nature, **269**:471–477.

McCook, L. J. 1999. Macroalgae, nutrients and phase shifts on coral reefs: scientific issues and management consequences for the great barrier reef. Coral reefs, **18**:357–367.

Meijer, M. L., E. Jeppesen, E. Van Donk, B. Moss, M. Scheffer, E. Lammens, E. Van Nes, J. Van Berkum, G. De Jong, B. Faafeng, et al. 1994. Long-term responses to fish-stock reduction in small shallow lakes: interpretation of five-year results of four biomanipulation cases in the netherlands and denmark. Hydrobiologia, **275**:457–466.

Nicholson, S. 2000. Land surface processes and sahel climate. Reviews of Geophysics, **38**:117–139.

Noy-Meir, I. 1975. Stability of grazing systems: an application of predator-prey graphs. The Journal of Ecology, pages 459–481.

Nyström, M., C. Folke, and F. Moberg. 2000. Coral reef disturbance and resilience in a human-dominated environment. Trends in ecology & evolution, **15**:413–417.

23

Reynolds, J. F., D. M. S. Smith, E. F. Lambin, B. Turner, M. Mortimore, S. P. Batterbury, T. E. Downing, H. Dowlatabadi, R. J. Fernández, J. E. Herrick, et al. 2007. Global desertification: building a science for dryland development. science, **316**:847–851.

Rietkerk, M. and J. van de Koppel. 1997. Alternate stable states and threshold effects in semi-arid grazing systems. Oikos, pages 69–76.

Rietkerk, M., F. van den Bosch, and J. van de Koppel. 1997. Site-specific properties and irreversible vegetation changes in semi-arid grazing systems. Oikos, pages 241–252.

Rinaldo, A., M. Gatto, and I. Rodríguez-Iturbe. 2020. River networks as ecological corridors: Species, populations, pathogens. Cambridge University Press.

Savage, V. M., J. F. Gillooly, J. H. Brown, G. B. West, and E. L. Charnov. 2004. Effects of body size and temperature on population growth. The American Naturalist, **163**:429–441.

Scheffer, M., S. Carpenter, J. A. Foley, C. Folke, and B. Walker. 2001. Catastrophic shifts in ecosystems. Nature, **413**:591–596.

Scheffer, M. and S. R. Carpenter. 2003. Catastrophic regime shifts in ecosystems: linking theory to observation. Trends in ecology & evolution, **18**:648–656.

Scheffer, M., S. H. Hosper, M. L. Meijer, B. Moss, and E. Jeppesen. 1993. Alternative equilibria in shallow lakes. Trends in ecology & evolution, **8**:275–279.

Scheffer, M., S. Rinaldi, A. Gragnani, L. R. Mur, and E. H. van Nes. 1997. On the dominance of filamentous cyanobacteria in shallow, turbid lakes. Ecology, **78**:272–282.

Stevens, V. M., S. Whitmee, J.-F. Le Galliard, J. Clobert, K. Böhning-Gaese, D. Bonte, M. Brändle, D. Matthias Dehling, C. Hof, A. Trochet, et al. 2014. A comparative analysis of dispersal syndromes in terrestrial and semi-terrestrial animals. Ecology letters, **17**:1039–1052.

Suding, K. N., K. L. Gross, and G. R. Houseman. 2004. Alternative states and positive feedbacks in restoration ecology. Trends in ecology & evolution, **19**:46–53.

24

Tamme, R., L. Götzenberger, M. Zobel, J. M. Bullock, D. A. Hooftman, A. Kaasik, and M. Pärtel. 2014. Predicting species' maximum dispersal distances from simple plant traits. Ecology, **95**:505–513. [466] [467] [468]

van de Koppel, J., M. Rietkerk, and F. J. Weissing. 1997. Catastrophic vegetation shifts and soil degradation in terrestrial grazing systems. Trends in Ecology & Evolution, **12**:352–356. [469] [470]

van de Leemput, I. A., E. H. van Nes, and M. Scheffer. 2015. Resilience of alternative states in spatially extended ecosystems. PloS one, **10**:e0116859. [471] [472]

van Nes, E. H. and M. Scheffer. 2005. Implications of spatial heterogeneity for catastrophic regime shifts in ecosystems. Ecology, **86**:1797–1807. [473] [474]

Walker, B. H. 1995. Rangeland ecology: managing change in biodiversity. In Biodiversity conservation, pages 69–85. Springer. [475] [476]

Wang, G. and E. A. Eltahir. 2000. Ecosystem dynamics and the sahel drought. Geophysical research letters, **27**:795–798. [477] [478]

Wilson, J. B. and A. D. Agnew. 1992. Positive-feedback switches in plant communities. Advances in ecological research, **23**:263–336. [479] [480]

Zelnik, Y. R., J.-F. Arnoldi, and M. Loreau. 2019. The three regimes of spatial recovery. Ecology, **100**:e02586. [481] [482]

Supplementary material

S1   Metapopulation model

We used a model of spatially structured population describing the dynamics of n patches linked by the dispersal of individuals. The dynamics of the biomass (x_i) inside the patch i are described by the following differential equation:

$$\frac{dx_i}{dt} = f(x_i) + g(x_i, x_.) \tag{2}$$

where $f(x_i)$ is a function describing the local dynamics of the patch and $g(x_i, x_.)$ describes the net dispersal between the patch i and its neighbors.

Local dynamics   We describe the local dynamics with a model coined by Noy-Meir (1975) that exhibits bistability and catastrophic shifts between a null-biomass state ($x_i = 0$) and a positive equilibrium ($x_i = x^*$) (Eq. 3). It describes the dynamics of a biotic resource x_i (*e.g.*, the biomass of plants) that grows logistically with a growth rate r and a carrying capacity K. This resource is harvested/consumed by a fixed consumer with a Holling type II functional response (with B the maximal harvesting rate and A the resource biomass at which the harvesting is half of B):

$$f(x_i) = rx_i \left(1 - \frac{x_i}{K}\right) - \frac{Bx_i}{A + x_i} \tag{3}$$

Although it was first coined to describe the dynamics of a plant biomass is a pasture grazed by herbivores (Noy-Meir, 1975), this model is fairly general as logistic growth is commonly used to model the growth of a wide range of organisms (but see Mallet (2012)), and type II functional responses are the norm for numerous consumers (Jeschke et al., 2004; Kalinkat et al., 2013). This system admits two tipping points ($B = AR$ and $B = Ar + K(1 - AK)/4$). It is bistable in this range ($AR < B < Ar + K(1 - AK)/4$) and admits two stable equilibria ($x_i = 0$ and $x_i = r_1$) separated by an unstable equilibrium ($0 < r_2 < r_1$).

26

Spatial dynamics   We consider that the individuals leave the patch i at a constant rate μ and are equally split between its neighbours. The patch also receives individuals from its neighbours in the same pattern which yields the following equation:

$$g(x_i, x.) = -\mu x_i + \mu \sum_{j \, adjacent \, i} \frac{x_j}{Ne_j}$$

where Ne_j is the number of neighbours of j.

503

Global dynamics of the system   The dynamics of the system are thus described by a system of n 504
coupled differential equations, which can also be written in a matricial form: 505

$$\frac{d\vec{x}}{dt} = r\vec{x}\left(1 - \frac{\vec{x}}{K}\right) - B\frac{\vec{x}}{A + \vec{x}} + \mu\, M\vec{x} \tag{4}$$

where $\vec{x}$ is the vector of local densities and M is a matrix describing the structure of the population: 506
the diagonal terms describe the emigration ($M_{ii} = -1$) and the off-diagonal terms the immigration   507
($M_{ij,i\neq j} = 0$ if i and j are not neighbors and $M_{ij,i\neq j} = 1/Ne_j$ if i and j are neighbors).   508

Two-patch system   The two patch system we used for the analytical stability analysis of a simple spatial system is a particular case of the model presented above, described by the following equations:

$$\frac{dx_1}{dt} = rx_1\left(1 - \frac{x_1}{K}\right) - \frac{Bx_1}{A + x_1} - \mu(x_1 - x_2)$$
$$\frac{dx_2}{dt} = rx_2\left(1 - \frac{x_2}{K}\right) - \frac{Bx_2}{A + x_2} - \mu(x_2 - x_1)$$

27

S2 Landscape design

We generated landscapes of $n = 100$ patches. We used four different landscape structures in order to explore the effect of space on catastrophic shifts: regular graphs (*e.g.*, patches arranged either linearly or on a lattice), Erdős–Rényi graphs (where patches are connected randomly), random geometric graphs (RGG, where patches are drawn randomly in space and connected depending on their distance) and optimal channel networks (that are generated using geomorphological processes). The main text analysis is made on networks where the patches have on average 4 neighbors each (when possible), and we conducted sensitivity analysis on the connectivity by generating networks with higher and lower connectivity (section S4).

Regular graphs   Regular graphs are graphs in which all nodes have the same number of neighbours: patches are either organized linearly on a cirlce (in 1-D) or on a regular lattice on a torus (for 2-D system). These graph have been used extensively for modelling explicit space (Keitt et al., 2001; van Nes and Scheffer, 2005), so we chose to use them for comparison with existing studies. They can be thought of as a null model of the most ordered spatial system possible. We used patches on a 10*10 lattice with periodic boundary conditions and connections to the 4 nearest neighbours for the main text. For the sensitivity analysis, we used patches on a 10*10 lattice with periodic boundary conditions and connections to the 8 nearest neighbours (2-D system, mean degree = 8) and 100 patches on a circle with connections to the 2 nearest neighbours (1-D system, mean degree = 2).

Erdős–Rényi graphs   Erdős–Rényi graphs are a class of graphs obtained by randomly connecting nodes: each pair of patches is connected with a probability p. The expected number of links per node (mean degree) is thus $p*(n-1)$ where n is the total number of patches. We used Erdős–Rényi graphs with $n = 100$ patches and a connection probability of $p = 4/(n-1)$ for the main text (expected mean degree $= 4$, realized mean degree $= 4$). For the sensitivity analysis, we used connection probabilities of $p = 8/(n-1)$ (expected mean degree $= 8$, realized mean degree $= 8$)

28

and $p = 2/(n-1)$ (expected mean degree = 2, realized mean degree = 2.7). After generating a 534 graph, we checked if it was connected (*i.e.*, that there existed at least an indirect path between all 535 pairs of nodes) and discarded the graphs that were not connected. 536

Random geometric graphs   Random geometric graphs (RGG) are obtained by drawing nodes 537 randomly in space and connecting the pair of nodes that are closer than chosen a threshold distance. 538 We generated each RGG by drawing 100 pairs of x and y coordinates uniformly in $[0, 1]$. We then 539 determined the threshold distance that yielded the average degree the closest to a target degree 540 (main text: target degree = 4; sensitivity analysis: target degree = 8). We once again checked if the 541 graphs were connected and discarded those that were not connected. Note that the connectivity of a 542 RGG is constrained by the initial drawing of coordinates, so it was not always possible to reach the 543 targeted average degree. RGGs connectivity deviated a bit from the regular graph counterpart (main 544 text: realized average degree = 4.7; realized degree = 7.9) 545

Optimal channel networks   Optimal channel networks are obtained by simulating geomorpholog- 546 ical processes and in order to capture the structural properties of riverine networks. We generated 547 OCN of $n = 100$ patches using the R-package OCNet (version 0.4.0) (Carraro et al., 2020). Be- 548 cause the structure of OCN is constrained by the underlying generating process and generally 549 scale-invariant, we could not manipulate the average degree of these networks (average degree = 550 1.98). 551

S3 Polynomial form of three classical desertification models

In this annex, we highlight the mathematical similarities between four classical models of bistable systems — three models of desertification taken from Noy-Meir (1975), Klausmeier (1999) and van de Koppel et al. (1997); and a model of logistic growth with an Allee effect. We argue that, despite the fact that they are built on different mechanistic processes, they behave similarly as they are all build from a simple third degree polynomial. In the first part, we conduct the exact stability analysis of this third degree polynomial. We then show in the subsequent parts how to relate models of desertification to this polynomial, and how it simplifies their stability analysis.

S3.1 Stability analysis of a dynamical model described by a third degree polynomial

The most straightforward way to model bistability is using a cubic polynomial to describe the evolution of a quantity (number of individuals, plant cover, share of users adopting a new technology...) in a closed system. Let us call P such a polynomial:

$$P \colon \mathbb{R} \to \mathbb{R}$$
$$x \mapsto \frac{dx}{dt} = \alpha_3 x^3 + \alpha_2 x^2 + \alpha_1 x + \alpha_0$$

Realistically, α_3 should be negative (otherwise $dx/dt \to \infty$ when x is high, meaning the population is unbounded). Hence, α_3 is restricted to negative values in what follows. In biological systems, realism also imposes a restriction on α_0: since the system is closed and x describes a density of organisms that cannot be spontaneously generated, $P(0)$ must be null, and hence $\alpha_0 = 0$. Additionally, x can only be positive when describing a population, so P only needs to be defined on $\mathbb{R}^+$.

Hereafter, P refers to the previously defined polynomial with these additional restrictions:

$$P \colon \mathbb{R}^+ \to \mathbb{R}$$

$$x \mapsto \frac{dx}{dt} = \alpha_3 x^3 + \alpha_2 x^2 + \alpha_1 x,$$

$$\alpha_3 < 0$$

Existence of alternative equilibria: Since $\alpha_0 = 0$, the system has an immediate equilibrium for $x = 0$. The other equilibrium can thus be found by solving:

$$\alpha_3 x^2 + \alpha_2 x + \alpha_1 = 0$$

This is a degree two polynomial with discriminant $\Delta = \alpha_2^2 - 4\alpha_3\alpha_1$. If $\Delta < 0$ (*i.e.* $4\alpha_3\alpha_1 > \alpha_2^2$), the polynomial has no real root and 0 is the only equilibrium of this system (Fig.S3.1c)

If $\Delta > 0$, then there are two other roots to the system (that are only relevant when they are positive):

$$r_1 = \frac{-\alpha_2 - \sqrt{\Delta}}{2\alpha_3}$$
$$r_2 = \frac{-\alpha_2 + \sqrt{\Delta}}{2\alpha_3}$$

The nature of the system depends on the sign of these roots: if both are negative, then 0 is a stable equilibrium and the only biologically significant equilibrium. If both are positive, 0 is still a stable equilibrium but there is also a stable positive equilibrium (r_1) separated from 0 by an unstable equilibrium (r_2) and thus the system is bistable (Fig. S3.1d). If only one of them is positive, then 0 is unstable and r_1 is stable and the only positive equilibrium (Fig. S3.1e).

562
563
564
565
566

31

Sign of r_1: Since α_3 is negative, r_1 is of the same sign as $\alpha_2 + \sqrt{\Delta}$. Thus, r_1 is positive iff $\alpha_2 > -\sqrt{\Delta}$

$$\Leftrightarrow \begin{cases} \alpha_2 > 0 \\ \\ or \\ \\ \begin{cases} \alpha_2 < 0 \\ \\ and \\ \\ 4\alpha_3\alpha_1 < 0 \end{cases} \end{cases}$$

Thus r_1 is only negative when $\alpha_2 < 0$ and $4\alpha_3\alpha_1 > 0$, *i.e.* in the top left corner of the $\alpha_2 - 4\alpha_3\alpha_1$ plane (Fig.S3.1a).

Sign of r_2: Similarly, the sign of r_2 is that of $\alpha_2 - \sqrt{\Delta}$. r_2 is positive iff $\alpha_2 > \sqrt{\Delta}$

$$\Leftrightarrow \begin{cases} \alpha_2 > 0 \\ \\ and \\ \\ 4\alpha_3\alpha_1 > 0 \end{cases}$$

r_2 is thus only positive in the top right corner of the $\alpha_2 - 4\alpha_3\alpha_1$ plane (FigS3.1a).

These results are summed up in Fig.S3.1:

- if α_1 is positive (crossed area in Fig.S3.1a), the system always reach a stable positive equilibrium (r_1, Fig.S3.1g)

- If α_1 is negative, the behaviour of the system depends on the relative values of α_2 and $4\alpha_1\alpha_3$: if $\alpha_2^2 > 4\alpha_1\alpha_3$ (white area in Fig.S3.1a), the system is bistable and can either reach 0 or a positive equilibrium (r_1) depending on its initial state (Fig.S3.1f). If $\alpha_2^2 < 4\alpha_1\alpha_3$, the system has no strictly positive equilibrium and necessarily goes to 0.

567

568

569

570

571

572

573

574

575

576

577

32

Stability analysis and interpretation: One way to make light of this is to see that α_1 drives the ⁵⁷⁸ system behaviour when x is close to 0 while α_2 and α_3 become more predominant at high x value, ⁵⁷⁹ thus: ⁵⁸⁰

- if α_1 is positive, P is positive when x is close to 0 and thus 0 is unstable. Since P is negative ⁵⁸¹ when x is high (because α_3 is negative), P necessarily becomes null once (and only once) for ⁵⁸² a $x > 0$ which is a stable equilibrium. ⁵⁸³

- If α_1 is negative, P is negative around 0 and thus 0 is a stable equilibrium. In that case, either ⁵⁸⁴ α_2 makes a positive contribution high enough (meaning $\alpha_2^2 > 4\alpha_1\alpha_3$) for P to reach 0 two ⁵⁸⁵ more times (because P ultimately decreases to $-infinity$ at high x) and the system is bistable ⁵⁸⁶ or α_2 contribution is not enough ($\alpha_2^2 < 4\alpha_1\alpha_3$) to bring P to 0 again and thus 0 is the only ⁵⁸⁷ equilibrium. ⁵⁸⁸

An intuitive way to sum these relationships is by looking at the α_2-$4\alpha_1\alpha_3$ plane (Fig. S3.1a): in ⁵⁸⁹ the area under the x-axis (in green), the system necessarily goes to a positive equilibrium. Over the ⁵⁹⁰ x-axis, the curve defined by $y = x^2$ separates two areas: on the left (in red) where 0 is the only stable ⁵⁹¹ equilibrium and the system goes to extinction. On the right (in orange), the system is bistable. By ⁵⁹² increasing α_2 (moving from left to right) or α_1 (moving from top to bottom), we drive the system ⁵⁹³ away from extinction and towards either a positively stable domain (in green) or a bistable domain ⁵⁹⁴ (in orange) respectively. ⁵⁹⁵

S3.2 Application to biological systems: ⁵⁹⁶

While some theoretical studies chose to use a third degree polynomial as a simple way to obtain ⁵⁹⁷ bistable dynamics, models rooted in biological mechanisms are rarely expressed as third degree ⁵⁹⁸ polynomials — because cubic terms cubic terms are hard to intuitively link to a process. Instead the ⁵⁹⁹ dynamics of biological systems (dx/dt, usually expressing biomass or species density) are often ⁶⁰⁰ expressed as a combination of: ⁶⁰¹
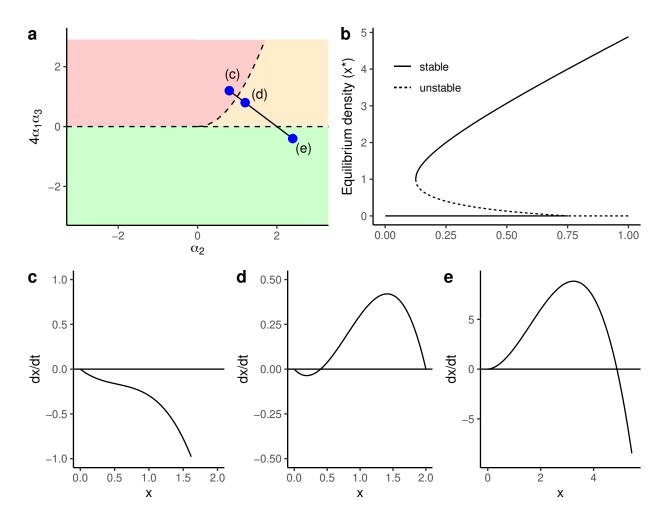
Figure S3.1: Description of P behaviour. **(a)** Phase diagram of P depending on α_2 and $4\alpha_3\alpha_1$. In the red area, 0 is the only equilibrium in $\mathbb{R}^+$ and the system always goes to extinction (see panel c). In the orange area, the system has three equilibrium in $\mathbb{R}^+$ ($[0, r_1, r_2]$) and goes either to extinction or r_2 depending on the initial x (see panel d). In the green area, 0 is an unstable equilibrium and the system always goes to r_1 that is stable (see panel e). The full line shows a transect happening when increasing both α_2 from 0.8 to 2.4 and α_1 from -0.6 to 0.2 (α_3 is fixed at -0.5) and the dots show where the panels c, c and e where taken. **(b)** bifurcation diagram (equilibria of $P(x)$) along the transect represented in the panel a (the x axis figures the position along the line: 0 is the point (c) and 1 is the point (e)). **(c)** a monostable parameterization of $P(x)$ resulting in extinction (parameters values of the point (c) in panel a: $\alpha_1 = -0.6$; $\alpha_2 = 0.8$; $\alpha_3 = -0.5$. **(d)** a bistable parameterization of $P(x)$ (parameters values of the point (d) in panel a: $\alpha_1 = -0.4$; $\alpha_2 = 1.2$; $\alpha_3 = -0.5$. **(e)** a monostable parameterization of $P(x)$ resulting in a positive equilibrium (parameters values of the point (e) in panel a: $\alpha_1 = 0.2$; $\alpha_2 = 2.4$; $\alpha_3 = -0.5$.
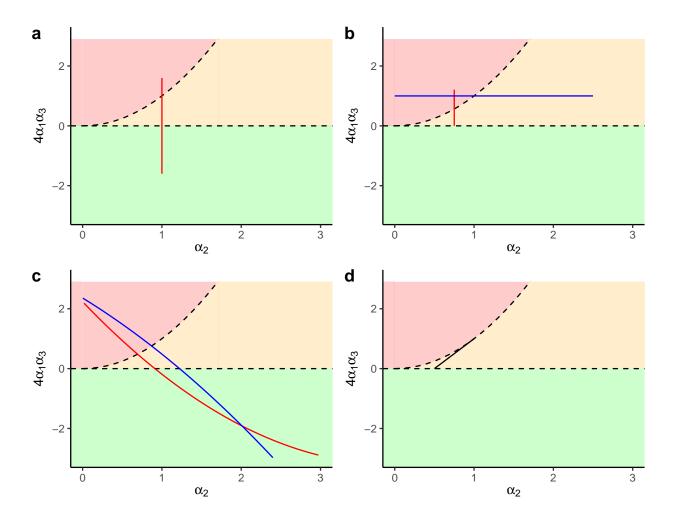
34

Figure S3.2: Situation of 4 classical models in the $alpah_2$-$\alpha_1\alpha_3$ plane (a: Noy-Meir, b: Klausmeier, c: Rietkerk and Van de Koppel, d: Logistic growth with an Allee effect). Red lines are transect obtained by varying mortality parameters, blue line are obtained by varying water input parameters. **(a)** Effect of varying the grazing pressure (B in 40-60) in the Noy-Meir model (other parameters: $r = 2$, $K = 50$, $A = 25$). **(b)** Effect of varying plant mortality (M in 0-1.1, red line) or the water input (A in 0-10, blue line) in the Klausmeier model (other parameters: $L = 0.5$, $R = 0.5$, $J = 0.5$; $A = 3$ for the red line and $M = 1$ for the blue line). **(c)** Effect of varying plant mortality (M in 0-0.1, red line) or the water input (I in 4-7, blue line) in the Rietkerk and Van de Koppel model (other parameters: $q = 0.1$, $L = 1$, $U = 1$, $R = 1$, $K = 10$, $A = 5$, $B = 5$; $I = 4$ for the red line and $M = 0.1$ for the blue line). **(d)** Effect of varying the Allee effect threshold (c in 0-1) in a logistic model with an Allee effect (other parameters: $r = 0.5$).

- linear terms ($\lambda * x$) to describe density independent processes (*e.g.*, death rate in birth-death processes, growth in an exponential model).

- square terms to describe density dependent processes such as mass action law (*e.g.*, intraspecific competition in a logistic growth model: $r(x - x^2/K)$).

- a quotient of low order polynomials (1 or 2) to describe saturating processes (*e.g.*, type 2 functional response: $n/(1 + n)$).

We found that a number of these models can be restated as a quotient of two polynomials:

$$f(n) := \frac{dx}{dt} = \frac{P(x)}{g(x)}$$

where P is the third degree polynomial described earlier and g is a strictly positive and monotonously increasing second order (at most) polynomial (defined on $\mathbb{R}^+$). Because of these properties, P and f share the same sign and roots despite f not being a polynomial. In the following section, we illustrate this using three classical models of desertification as well as a model of logistic growth with an Allee effect. We argue that: *i)* the stability analysis of these models is made much easier by mapping f to P and using the stability analysis of P, for which we know the exact expression and nature of its equilibria; *ii)* that expressing the parameters of P (α_1, α_2 and α_3) as aggregates of the parameters of f helps to understand the effect of biological parameters on the systems equilibria — in particular through the graphical analysis of the α_2-$\alpha_1\alpha_3$ plane — and *iii)* that the models we consider all share a common structure despite the fact that they describe different mechanistic processes, which is encouraging for the transposability of studies made on one of these models.

S3.2.1 Noy-Meir model

The model we use in the main text of this study describes the dynamics of plants (whose biomass is written x) grazed by a constant population of consumer (whose maximal grazing rate is B), as coined by Noy-Meir (1975). The variations of plant biomass are expressed by the following differential

equation:

$$\frac{dx}{dt} := f(n) = rx\left(1 - \frac{x}{K}\right) - \frac{Bx}{A+x} \tag{5}$$

In the absence of grazing, the plant biomass grow logistically with a growth rate r up to a carrying capacity K (left term). On top of that, a fixed consumer harvest the plant population following a Holling type 2 harvesting rate (right term) where B is the maximal harvesting rate and A is the biomass of plants at which the per plant biomass harvesting rate is half of its maximal value (half-saturation constant of the grazers): the grazing increases linearly with x at low plant biomass then reaches a plateau as each harvesting agent reaches its maximal harvesting rate.

Polynomial form: We rewrite $f(x)$ as a quotient of polynomial:

$$f(x) = \frac{\frac{-r}{K}x^3 + r(1 - A/K)x^2 + (Ar - B)x}{A + x} = \frac{P(x)}{g(x)}$$

Hence the coefficients of $P(x)$ are:

Coefficient	Expression
α_1	$Ar - B$
α_2	$r(1 - A/K)$
α_3	$-r/K$

Table S3.1: Coefficient of the polynomial $P(x)$ describing the behaviour of the Noy-Meir model.

The main control parameter — grazing intensity (B) — is only found in α_1. Varying this parameter moves the system vertically in the α_2-$4\alpha_1\alpha_3$ plane (Fig. S3.2a): it goes from the domain with a single positive equilibrium (green area) to the domain with a single null equilibrium (extinction, red area) through the bistable domain (orange area) as B increases. Note that in the unlikely case where $A > K$ (*i.e.*, the grazing saturates at a biomass level greater than the carrying capacity), α_2 is negative so the system goes from a positive biomass to extinction without going through a bistable phase as B increases.

S3.2.2 Klausmeier model

This model coined by Klausmeier (1999) and describes catastrophic shifts in arid grassland, but here the bistability arises from positive feedbacks between plant biomass (x) and water availability (w):

$$\frac{dw}{dt} = A - Lw - Rwx^2$$
$$\frac{dx}{dt} = RJwx^2 - Mx$$

with the following paramters:

- A the water input

- L the water loss rate

- R the rate at which plants uptake water

- J a conversion rate from water mass to plant biomass (*i.e.*, how much plant biomass is created from 1 unit of water mass).

- M the plant mortality rate.

The water dynamics depend on a constant water input (A, *e.g.*, the precipitation rate), water losses that are proportional to the amount of available water (Lw, *e.g.*, evaporation and infiltration in deep soil layers) and a water uptake by plants (Rwx^2) that is proportional to both the amount of proportional to the amount of available water and the square of plant biomass (the square term representing the facilitation between plants allows the system to be bistable). The plant dynamics are described by a growth term that is proportional to the water uptake ($RJwx^2$) and a death rate proportional to plant biomass (Mx).

It is common to assume that water dynamics are way faster than plant dynamics in models describing

plant-water dynamics. We can thus calculate the water equilibrium w^* by solving the equation $\dfrac{dw}{dt} = 0$:

$$w^* = \frac{A}{L + Rx^2}$$

By replacing w by its equilibrium w^* in the expression of water dynamics, we can describe the system using a single equation:

$$\frac{dx}{dt} := f(x) = \frac{RJAx^2}{L + Rx^2} - Mx$$

Polynomial form: Similarly to the Noy-Meir model, we can rewrite the equation above as a quotient of polynomials:

$$f(x) = \frac{-RMx^3 + ARJx^2 - LMx}{L + Rx^2} = \frac{P(x)}{g(x)}$$

The coefficients of $P(x)$ are:

Coefficient	Expression
α_1	$-LM$
α_2	ARJ
α_3	$-RM$

Table S3.2: Coefficient of the polynomial $P(x)$ describing the behaviour of the Klausmeier model.

The two main control parameters here are the plant mortality (M) and the water input (A). The plant mortality is only present in the $alpha_1$ and $alpha_3$ so — similarly to the Noy-Meir model — varying M moves the system vertically in the α_2-$4\alpha_1\alpha_3$ plane (Fig. S3.2b): it goes from the frontier between the domain with a single positive equilibrium (green area) and the bistable domain (orange area) to the domain with a single null equilibrium (extinction, red area) as M increases. The water input parameter (A) is only present in α_2, so varying it moves the system horizontally in the α_2-$4\alpha_1\alpha_3$ plane (Fig.S3.2b): increasing A moves the system from the red domain (monostable, extinction) to the orange domain (bistable).

Note that for this model, α_1 and α_3 are always negative (hence $4\alpha_1\alpha_3$ is always positive) and α_2

is always positive. Thus the system is necessarily in the top-right quadrant of the α_2–$4\alpha_1\alpha_3$ plane and thus is either bistable or admits only the null equilibrium (it cannot reach the green domain in the α_2–$4\alpha_1\alpha_3$ plane).

S3.2.3 Rietkerk & Van de Koppel model

The third model of desertification that we examine was coined van de Koppel et al. (1997) and also describes the dynamics of soil water (W) and plant biomass (x):

$$\frac{dw}{dt} = I\frac{x+Aq}{x+A} - Lw - Uwx \quad \frac{dx}{dt} = rx(1-x/K)\frac{w}{w+B} - Mx$$

Water (w) enters the soil through an infiltration facilitated by plants presence ($I(x+As)/(x+A)$, with I the water input) and exits it through abiotic losses ($-LW$) and plant uptake ($-Uwx$). The plants (x) grow following a logistic term ($rx(1-x)/K$) multiplied by a saturating function of w ($w/(w+B)$) describing how water affects plant growth; and they lose biomass at a constant rate M ($-Mx$). Similarly to the Klausmeier model, we can find the water equilibrium w^* by solving $dw/dt = 0$:

$$w^* = \frac{I(x+Aq)}{(L+Ux)(x+A)}$$

We can inject this equilibrium (under the assumption that water dynamics are faster than plant dynamics) into the expression of dx/dt to find:

$$\frac{dx}{dt} := f(x) = rx\left(1 - \frac{x}{K}\right)\frac{w^*}{w^*+B} - Mx$$

Polynomial form: By developing this expression, we find that it is once again a quotient of polynomials:

$$f(x) = \frac{P(x)}{g(x)}$$

with:

$$g(x) = A(Iq + BL) + x(I + B(L + AU)) + x^2 BU$$

and:

$$P(x) = x^3(-Ir/K - MBU) + x^2(Ir(1 - Aq/K) - IM - MBL - MBUA) + x(IAq(r - M) - MBAL)$$

whose coefficients are:

Coefficient	Expression
α_1	$IAq(r - M) - MBAL$
α_2	$Ir(1 - Aq/K) - IM - MBL - MBUA$
α_3	$-Ir/K - MBU$

Table S3.3: Coefficient of the polynomial $P(x)$ describing the behaviour of the model described by Rietkerk and Van de Koppel.

This model is a bit more complicated than the previous ones and would warrant a lengthy analysis of all its parameters and how they affect the systems equilibria. However, we will here focus on two simple results:

Firstly, the polynomial form provides a simple way to analyse the system: while the model uses 9 parameters, we can reduce the complexity of its analysis through the three compound parameters α_1, α_2 and α_3. For any set of parameters, it is easy to compute the *alpha* and then *i)* to determine the number and nature of the equilibria through the α_2-$4\alpha_1\alpha_3$ plane (Fig. S3.2c) and *ii)* to determine the exact values of these equilibrium through the analytical expresions of r_1 and r_2 that we derived in the section S3.1.

Secondly, we can analyze the impact of varying a given parameter using the α_2-$4\alpha_1\alpha_3$ plane. For the set of parameters used in Fig. S3.2c, we can see that the two control parameters (mortality rate

41

M and water input *I*) have a similar effect on the system. The system moves from a stable positive 690
equilibrium (green area) towards extinction (red area) through a bistable state (orange area) when 691
increasing the mortality (*M*, red line in Fig. S3.2c) or decreasing the water input (*I*, blue line). 692

S3.2.4 Logistic growth with an allee effect 693

Lastly, we focus on the model of a logistic growth with an Allee effect. For simplicity, we use a 694
model where *x* represents the species density rescaled to the carrying capacity (*i.e.*, *x* is the species 695
density in proportion of the carrying capacity). This system is described by the following equation: 696

$$\frac{dx}{dt} = rx(1-x)(x-c)$$

where *r* is the growth rate and *c* is the Allee effect threshold, *i.e.*, the density under which the 697
species growth is negative. 698

Polynomial form: Here, the equation describing the system is already a third degree polynomial 699
(*e.g.*, g(x) = 1) that we can express by developing the expression above: 700

$$\frac{dx}{dt} = -rx^3 + y^2 r(1+c) - rcy$$

Hence the coefficients of the polynomial form are: 701

Coefficient	Expression
α_1	$-rc$
α_2	$r(1+c)$
α_3	$-r$

Table S3.4: Coefficient of the polynomial $P(x)$ describing a logistic growth with an Allee effect.

Because this model is very simple by design, the polynomial analysis is not very useful here. It 702
is however interesting to note that it fits into the same framework as the more mechanistic models 703
presented above. The figures S3.2d shows how this model is situated in the $\alpha_2\text{-}4\alpha_1\alpha_3$ plane as *c* 704
varies. 705

42

S4   Sensitivity analysis on network connectivity 706

We conducted a sensitivity analysis on network conductivity by conducting the same simulations 707
as in the main text but on networks with higher or lower connectivity (see S2 for the generating 708
methods). We generated regular graphs where each patch had exactly 2 or 8 neighbours, which 709
respectively results in 100 patches on a circle with connections to the 2 nearest neighbours (1-D 710
system, mean degree = 2) and a 10*10 lattice with periodic boundary conditions and connections to 711
the 8 nearest neighbours (2-D system, mean degree = 8). We generated Erdös-Rényi graphs with a 712
target connectivity of 2 or 8, but because we constrained them to be connected graphs, this resulted 713
in an average connectivity slightly higher than 2 (2.7 on average) for the low connectivity networks. 714
We also generated RGGs with a target connectivity of 8 (which resulted in a realized connectivity 715
of 7.9 on average), but couldn't make RGGs with a lower connectivity than in the main text because 716
of constraints on the generating process. 717

S4.1   General patterns 718

The general patterns observed in the main text stayed qualitatively unchanged (Fig. S4.1 and S4.2): 719
hysteresis size first decrease with dispersal rate (until $\mu \sim 0.1$) and then increased to a plateau. 720
The effect of landscape type on hysteresis was conserved for highly connected graphs (regular 721
graphs > Erdös-Rényi graphs > RGGs, fig. S4.2) We suspect that this is due to differences in 722
degree distributions: in regular graphs, all patches have the same degree (4 or 8 neighbours), which 723
explains their larger hysteresis. Erdös-Rényi networks and RGGs have some variance in their node 724
degrees, so the perturbations were likely to happen on a low degree node and to initiate a large scale 725
shift, explaining their hysteresis size in between that of regular graphs and of OCNs. The difference 726
between RGGs and Erdös-Rényi graphs could be also due to differences degree distribution: while 727
they have a similar average degree, RGGs have a wider degree distribution, making it more likely 728
that a pertubation happens on a low-degree node than in Erdös-Rényi graphs, hence their smaller 729
hysteresis. 730

43

Hysteresis size was similar accross landscapes types for lowly connected graphs (Fig. S4.1), which 731
we conjecture is due to the very low degree heterogeneity at low connectivity. 732

733

Lastly, hysteresis size was smaller in less connected networks (Fig. S4.1) and higher in more 734
connected networks (Fig. S4.1), which is consistent with our interpretation that biomass dilution in 735
highly connected networks prevent the spread of local shifts. 736

S4.2   Perturbation modality 737

Lastly, the effect of perturbation modality was similar to what we observe in the main text. Targeting 738
clustered patches resulted in a smaller hysteresis than targeting patches dispersed over the landscape 739
in both lowly and highly connected networks (Fig. S4.3 and S4.4). 740

Targeting high or low degree node had only a marginal effect in lowly-connected Erdös-Rényi 741
networks and no effect otherwise (Fig. S4.5 and S4.6), similarly to what we observed in 4-degree 742
networks. 743

Figure S4.1: **Sensitivity analysis: networks with an average degree of 2.** Characterization of the large scale dynamics for different spatial structures of metapopulation (purple: circular network; green: Erdös-Rényi graphs). (a) Size of the hysteresis (computed as the area between the upper and lower branches of the bifurcation diagram of the average biomass) as a function of the dispersal rate. (b) and (c) large scale tipping points as a function of the dispersal rate: value of the harvesting rate (B) at which the system loses (b) or gains (c) the most biomass. All quantities are computed as the mean (full line) and standard deviation of 50 replicates.
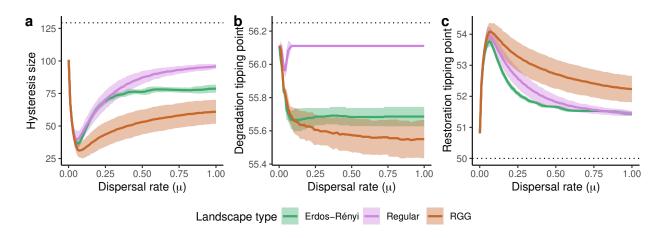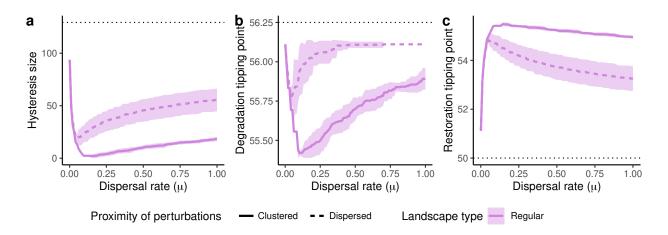
Figure S4.2: **Sensitivity analysis: networks with an average degree of 8.** Characterization of the large scale dynamics for different spatial structures of metapopulation (purple: regular grid; green: Erdös-Rényi graphs; brown: random geometric graphs). (a) Size of the hysteresis (computed as the area between the upper and lower branches of the bifurcation diagram of the average biomass) as a function of the dispersal rate. (b) and (c) large scale tipping points as a function of the dispersal rate: value of the harvesting rate (B) at which the system loses (b) or gains (c) the most biomass. All quantities are computed as the mean (full line) and standard deviation of 50 replicates.
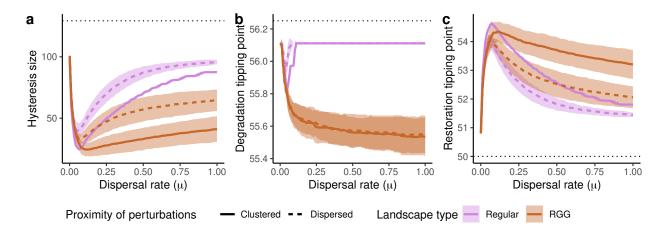

Figure S4.3: **Sensitivity analysis: networks with an average degree of 2.** Characterization of the large scale dynamics for different types of perturbations (full line: clustered perturbations, dashed lines: dispersed perturbations) and different spatial structures of metapopulation (purple: circular network). (a) Size of the hysteresis as a function of the dispersal rate. (b) and (c) large scale tipping points as a function of the dispersal rate: value of the harvesting rate (B) at which the system loses (b) or gains (c) the most biomass. All quantities are computed as the mean (lines) and standard deviation of 50 replicates.
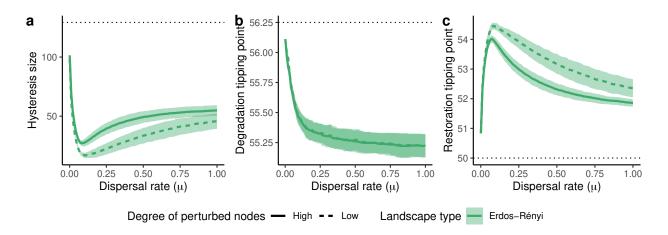
Figure S4.4: **Sensitivity analysis: networks with an average degree of 8.** Characterization of the large scale dynamics for different types of perturbations (full line: clustered perturbations, dashed lines: dispersed perturbations) and different spatial structures of metapopulation (purple: regular grid). (a) Size of the hysteresis as a function of the dispersal rate. (b) and (c) large scale tipping points as a function of the dispersal rate: value of the harvesting rate (B) at which the system loses (b) or gains (c) the most biomass. All quantities are computed as the mean (lines) and standard deviation of 50 replicates.

Figure S4.5: **Sensitivity analysis: networks with an average degree of 2.** Characterization of the large scale dynamics for different types of perturbations (full line: perturbation of high-degree nodes, dashed lines: perturbation of low-degree nodes) and different spatial structures of metapopulation (green: Erdös-Rényi graphs). (a) Size of the hysteresis as a function of the dispersal rate. (b) and (c) large scale tipping points as a function of the dispersal rate: value of the harvesting rate (B) at which the system loses (b) or gains (c) the most biomass. All quantities are computed as the mean (lines) and standard deviation of 50 replicates.
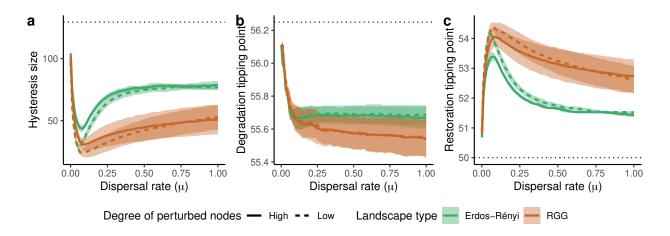
Figure S4.6: **Sensitivity analysis: networks with an average degree of 8.** Characterization of the large scale dynamics for different types of perturbations (full line: perturbation of high-degree nodes, dashed lines: perturbation of low-degree nodes) and different spatial structures of metapopulation (green: Erdös-Rényi graphs; brown: random geometric graphs). (a) Size of the hysteresis as a function of the dispersal rate. (b) and (c) large scale tipping points as a function of the dispersal rate: value of the harvesting rate (B) at which the system loses (b) or gains (c) the most biomass. All quantities are computed as the mean (lines) and standard deviation of 50 replicates.

S5   Analysis of a two-patch system

744

At high dispersal (Fig. S5.1 a, b & c), the densities at equilibrium are the same in the two patches 745 because of the strong homogenization between patches: all equilibria are situated on the $x_1 = x_2$ 746 plane. Spatial bistability — the stable coexistence of a high- and low-biomass states in the two 747 patches — is not possible, and biomass differences between the two patches can only exist as a 748 transient state towards an homogeneous stable state. The whole system behaves as a single bistable 749 unit with two stable equilibria $((x_1, x_2) = (0,0)$ and $(x_1, x_2) = (r_1, r_1))$ separated by an unstable 750 equilibrium $((x_1, x_2) = (r_2, r_2))$ over the same range of harvesting rate as for an isolated patch 751 $(50 < B < 56.25)$. 752

   As dispersal decreases, the equilibria on the $x_1 = x_2$ plane keep their values and nature, but 753 branches appear outside of the $x_1 = x_2$ plane at high harvesting rates *(right before the tipping point* 754 *toward the desert equilibrium)* (Fig. S5.1 d, e & f). These branches appear from the unstable branch 755 $((x_1, x_2) = (r_2, r_2))$ that separates the desert equilibrium $((x_1, x_2) = (0,0))$ from the vegetated 756 equilibrium $((x_1, x_2) = (r_1, r_1))$ and are themselves unstable. At really low dispersal, spatial 757 bistability becomes possible (meaning the coexistence of patches with different plant biomasses in 758 the metacommunity) since part of the branches outside the $x_1 = x_2$ plane become stable (Fig. S5.1 759 g, h & i). These new stable equilibria are associated with strong differences in biomass between the 760 two patches, with one patch at a biomass really close to r_1 while the other is close to 0. 761
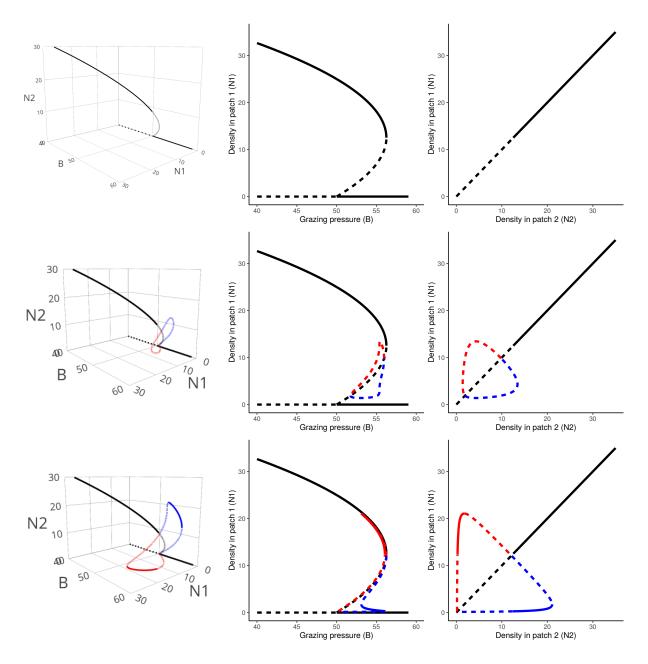
48

Figure S5.1: Bifurcation diagrams of a system of two patches connected through dispersal for various dispersal rates: $\mu = 0.3$ (top row), $\mu = 0.03$ (middle row) and $\mu = 0.005$ (bottom row); diagrams in the $n_1 - n_2 - B$ space (density in both patches 1 and 2, grazing pressure) in the left column, and their projections on the $B - n_1$ plane (middle column) and $n_1 - n_2$ plane (right column). Continuous lines depict stable equilibria and dotted lines unstable ones. The branches in black are in the $n_1 = n_2$ plane (equal densities in both patches), the colored branches are outside of this plane.

S6   Supplementary figures and tables referenced in the main text

762

763

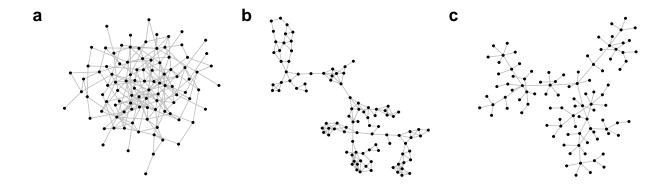| Parameter	Value	Biological meaning
r	2	resource growth rate
K	50	resource carrying capacity
A	25	half saturation of harvesting

Table S6.1: Constant parameters used for the Noy-Meir model.

Figure S6.1: Examples of three landscapes used in the main text analysis. (a) An Erdös-Rényi graph, (b) a random geometric graph (RGG) and (c) an optimal chanel network (OCN).
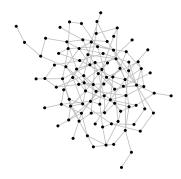

Figure S6.2: Examples of a low-connectivity Erdös-Rényi graph used in the sensitivity analysis.
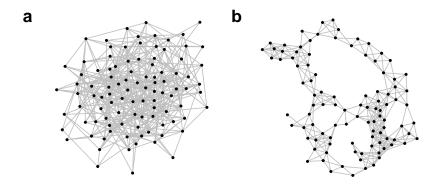
50

Figure S6.3: Examples of two high-connectivity landscapes used in the sensitivity analysis. (a) An Erdös-Rényi graph, (b) a random geometric graph (RGG).